

SOLAR-LIKE OSCILLATIONS IN A METAL-POOR GLOBULAR CLUSTER WITH THE HST*

DENNIS STELLO¹, RONALD L. GILLILAND²

Draft version November 21, 2018

ABSTRACT

We present analyses of variability in the red giant stars in the metal-poor globular cluster NGC6397, based on data obtained with the *Hubble Space Telescope*. We use a non-standard data reduction approach to turn a 23-day observing run originally aimed at imaging the white dwarf population, into time-series photometry of the cluster's highly saturated red giant stars. With this technique we obtain noise levels in the final power spectra down to 50 parts per million, which allows us to search for low amplitude solar-like oscillations. We compare the observed excess power seen in the power spectra with estimates of the typical frequency range, frequency spacing and amplitude from scaling the solar oscillations. We see evidence that the detected variability is consistent with solar-like oscillations in at least one and perhaps up to four stars. With metallicities two orders of magnitude lower than of the Sun, these stars present so far the best evidence of solar-like oscillations in such a low metallicity environment.

Subject headings: stars: fundamental parameters — stars: oscillations — stars: interiors — techniques: photometric — open clusters and associations: individual: NGC6397

1. INTRODUCTION

Theoretical models predict that cool stars with convective envelopes exhibit oscillatory motion due to excitation of a large number of eigen modes by the turbulent gas motion near the surface. The resulting p-mode oscillations are standing sound waves with the restoring force being pressure, hence their name, which therefore depend on the internal structure of the star. For historical reasons these oscillations are also known as solar-like oscillations. The technique of analyzing these oscillations to infer and constrain the stellar properties, called Helioseismology when applied to the Sun, has shown some remarkable results over the last few decades, and is starting to show promising results when applied to other stars – known as asteroseismology, e.g. see Bedding & Kjeldsen (2007) and references therein.

A typical characteristic of p-mode oscillations is an almost equidistant frequency spacing between modes of successive radial order with a broad, smoothly varying amplitude profile as a function of frequency. Amplitudes are only a few tens of centimeters per second in velocity and a few parts per million (ppm) in intensity in stars similar to the Sun, while the more vigorous convection in red giant stars generate amplitudes much larger, reaching up to several meters per second or the order of 1000 ppm (~ 1 mmag) in intensity. The higher signal-to-noise and prospects of obtaining additional measures to constrain the stellar parameters at this interesting evolutionary state makes red giants obvious targets for asteroseismic study.

A few simple relations exist to predict the ampli-

tude, frequency, and frequency spacing of p-mode oscillations. There is quite strong observational evidence that the typical frequency range of the oscillations scales with the acoustic cut-off frequency (Kjeldsen & Bedding 2004; Stello et al. 2008), as suggested by Brown et al. (1991). There is also good agreement between the observed frequency spacings and those predicted by scaling the square root of the stellar density Kjeldsen & Bedding (1995); Kjeldsen et al. (2008b). However, there is less of an agreement when it comes to the amplitude of the modes, which might be related to the often unknown mode lifetime. Kjeldsen & Bedding (1995) suggested that the amplitude per mode would be proportional to the luminosity-to-mass ratio in velocity and $LM^{-1}T_{\text{eff}}^{-2}$ in intensity. This was based on measured amplitudes from various types of oscillating stars. More recent theoretical studies by Samadi et al. (2005) indicate that $(L/M)^{0.7}T_{\text{eff}}^{-2}$ in intensity might be a better scaling factor.

Oscillations have now been clearly detected in a few bright red giant field stars, both in velocity (Frandsen et al. 2002; De Ridder et al. 2006; Hatzes & Zechmeister 2007) and photometry (Barban et al. 2007). While earlier datasets were not adequate to clearly establish the p-mode nature of the detected variability, the more recent measurements leave little or no doubt as the reality of p-mode oscillations in red giants. However, there is still no clear consensus on the mode lifetimes, and it is still not well known to what extent non-radial modes are present. For the star ξ *Hya* Stello et al. (2006) found a mode lifetime of a few days assuming only radial modes, which was significantly shorter than the theoretical value of about 17 days derived by Houdek & Gough (2002). Similarly for ϵ *Oph*, Barban et al. (2007) also found a short mode lifetime assuming only radial modes, while Kallinger et al. (2008a) used the same photometry to conclude that this star showed both radial and non-radial pulsations with mode lifetimes of roughly 10-20 days.

After indications of p-mode oscillations were obtained in a large sample of red giant stars from a 38-h run on

¹ Sydney Institute for Astronomy (SifA), School of Physics, University of Sydney, NSW 2006, Australia; stello@physics.usyd.edu.au.

² Space Telescope Science Institute, 3700 San Martin Drive, Baltimore, Maryland 21218, USA; gillil@stsci.edu.

* Based on observations with the NASA/ESA Hubble Space Telescope, obtained at the Space Telescope Science Institute, which is operated by the Association of Universities for Research in Astronomy, Inc., under NASA contract NAS 5-26555.

the globular cluster 47 Tuc ($[\text{Fe}/\text{H}] \simeq -0.7$) with the *Hubble Space Telescope* (HST) (Edmonds & Gilliland 1996), large efforts have been made to detect p-mode oscillations in stellar clusters based on extended ground-based photometry. The open cluster M67 ($[\text{Fe}/\text{H}] \simeq 0.0$) has so far only provided marginal detections in a few red giants (Gilliland et al. 1993; Stello et al. 2007). The results by Stello et al. (2007) showed slightly better agreement with the $LM^{-1}T_{\text{eff}}^{-2}$ scaling than the $(L/M)^{0.7}T_{\text{eff}}^{-2}$ scaling. However, no strong conclusions could be drawn because the extent to which non-radial modes were present could not be established. Aimed at the red giant population of the metal-poor globular cluster M4 ($[\text{Fe}/\text{H}] \simeq -1.2$) Frandsen et al. (2007) were only able to establish upper limits on the amplitudes, which were not in agreement with the $LM^{-1}T_{\text{eff}}^{-2}$ scaling, but still consistent with the more modest estimates from the $(L/M)^{0.7}T_{\text{eff}}^{-2}$ scaling. Frandsen et al. (2007) suggested the lower amplitudes in M4 relative to M67 could be due to its lower metallicity. This is supported by the velocity measurements of the subgiant field star ν Ind by Bedding et al. (2006), which is the most metal-poor star ($[\text{Fe}/\text{H}] \simeq -1.4$) for which p-mode oscillations have been detected so far.

In this paper we aim to detect p-mode oscillations from a group of red giants in the metal-poor globular cluster NGC6397 ($[\text{Fe}/\text{H}] \simeq -2.0$; Richer et al. (2008)) from 23 days of photometry from the HST, and use those results to test the scaling relations for the mode amplitudes. First, we give a detailed description of the non-standard data reduction that was required for this investigation in § 2. Then, in § 3 we provide the derivation of stellar parameters and estimated asteroseismic characteristics, which leads to the time-series analysis in § 4, and estimates of the mode amplitudes in § 5. In § 6 we search for a regular pattern in the power spectrum of the time series, and discuss our results in § 7. Finally, we give the conclusions in § 8.

2. OBSERVATIONS OF NGC6397

The data on the red giants presented in this paper were serendipitously obtained as part of GO-10424 (Richer et al. 2008), a program executed over 2005 March 17 – April 9 during 126 orbits with the HST’s ACS/WFC (Cycle 13). While the original program aimed to probe the bottom of the white dwarf cooling sequence of NGC 6397 through deep imaging of a single field in this nearby globular cluster (Hansen et al. 2007), we use the 363 exposures as one 23-day time series to allow detection of stellar variability. During each 96-minute orbit, typically one exposure through the F606W filter was obtained, which was bracketed by two exposures through the F814W filter separated by roughly 16 minutes. Figure 1 shows the time series of one of the stars. The exposure times were on average 713 seconds for F606W and 742 seconds for F814W. However, the data acquisition was not optimized for our purpose, the red giants were saturated, and images were dithered over several pixels – both effects adding noise to the final time series.

Due to saturation we had to abandon PSF fitting for the target stars, and instead use aperture photometry. The goal of the following step was to find an aperture mask, as small as possible, for each star that would always encompass all of the pixels that were ever bled into for the over-saturated stars. We first formed a stack of

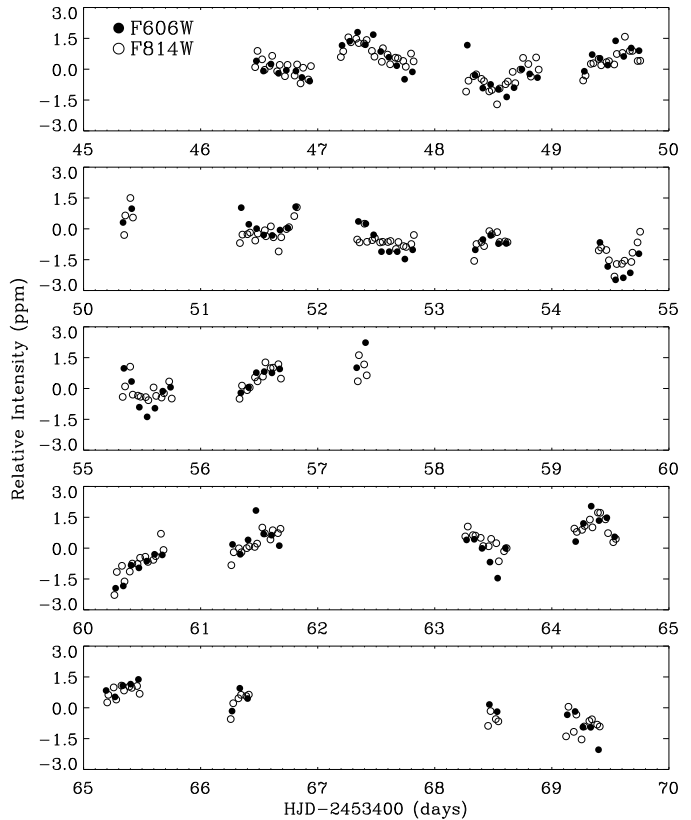


FIG. 1.— Time series of the brightest cluster member (No 1) on the WFC1 chip. During this 23 day period 37% of all HST orbits had data for this project, and within orbits 38% duty cycle was achieved.

the longest exposures after shifting them to a common x, y position. The frame-to-frame offsets were found by fitting PSFs to 42 non-saturated stars in each image, and solving for offsets, rotation, and plate scale changes relative to an overall mean. Then, for each pixel in the stack we looked at the distribution of counts, and assigned the pixel to be part of the aperture if there was more than one value in the distribution near the known saturation threshold of the chip. In case there was only one value near saturation it would more likely be due to a cosmic ray event, and was ignored to avoid spuriously large apertures. This was done separately for the two filters, and was based on 84 exposures of 769 seconds in F606W and 93 exposures of 804 seconds in F814W, the longest exposure time used for either filter. We were now able to extract simple aperture photometry for the 510 brightest stars on chip WFC1 that did not bleed off the edges. This included 255 stars that were slightly saturated (bleeding never exceeded a radius of 3 pixels), and 255 stars with significant saturation. For the brightest star the aperture contained slightly more than 10,000 pixels and was nearly 1700 pixels tall along the bleeding direction. Due to small number statistics only one of the two chips – WFC1 – contained stars suitable for this investigation which is aimed at red giants with the F814W magnitude $\lesssim 13$.

To reduce the spurious noise introduced by the dithering we decorrelated the time series with a large number of external parameters. For previous experiments with HST data where the dithering had been within ± 0.5 pixels, the primary decorrelation vectors were simply the x, y offsets frame-to-frame (Gilliland 2008). For these observations the dithering placed equal amounts of data in 10 widely separated pixels, with data points within each position uniformly distributed in time. In examining the raw time series it was obvious that unique offsets in the photometry often existed for one (or more) of these offset positions. We remove those offsets by decorrelating with nine independent vectors while adjusting to a common zero point corresponding to the 10th dither position. For most time series linear correlation coefficients remained small for most terms. But, sometimes when photometric offsets unique to a dither position existed, the correlation could be larger than 0.9.

Within each dither position there were additional sub-pixel offsets which varied up to ± 0.25 pixels. These tended to be along an x, y diagonal. Hence we formed 10 additional vectors – one for each dither position – to remove photometry variations that correlated with the sub-pixel offsets. Again, it was usually the case that linear correlations between these sparsely populated vectors and the photometry were small.

We included a total of four more decorrelation vectors: (1) a median over the 510 input stars to enforce an ensemble mean; (2) the local sky value frame-to-frame to correct any systematic errors in the initial sky subtraction; (3) the frame-to-frame exposure time to correct non-linearities; (4) and a goodness of fit parameter from the earlier step of fitting PSFs to deal with any focus changes. Again, most correlations remained small, but occasionally a star would see dramatic improvement from one of these terms. The decorrelations were performed iteratively with allowance for dropping points for which deviations were larger than 4σ . Over the 242 frames in F814W and 121 frames in F606W an average of 4.4 points and 1.4 points were removed, respectively.

To test that the large number of decorrelation parameters (24 in total) did not wreak havoc with the data, we performed the following experiment. Starting with the original non-decorrelated time series for the 510 stars we injected sinusoidal signals with amplitudes of 0.001 and frequencies that uniformly spanned 1 to $100\mu\text{Hz}$, after which we decorrelated the resulting time series. Separately, we injected the same set of sinusoids in the original data after decorrelation, and then compared signals between the two. This comparison showed that our decorrelation process made almost no difference for the injected sinusoids at any frequency.

Overall, the final time series rms remains about 50% above the Poisson limit in the stars that are slightly saturated, to a factor of two above for more strongly saturated stars, as illustrated in Figure 2. The inability to eliminate most cosmic rays in these heavily saturated stars can explain much of this excess residual. Among the red giant stars we see additional excess rms, which is likely intrinsic stellar variability.

3. STELLAR PARAMETERS

Within the 510 stars we used Table 1 of Richer et al. (2008) to select all of the proper motion cluster members

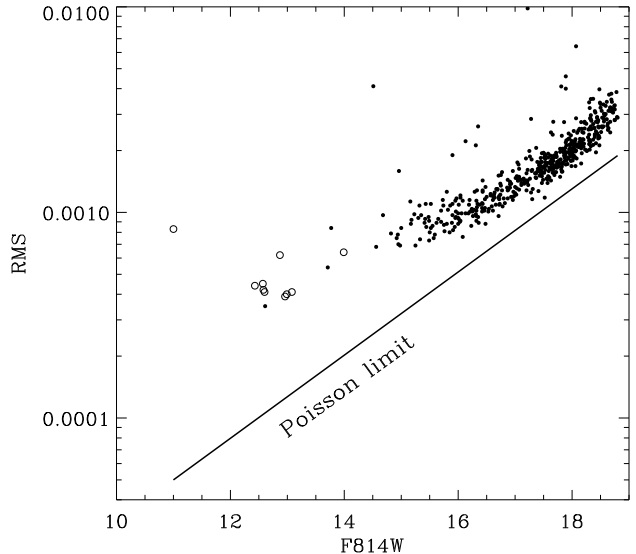


FIG. 2.— Standard deviation of time series as a function of magnitude for all 510 stars examined. Open circles show the 10 brightest cluster members listed in Table 1. All 510 stars are saturated, which explains their rms offset relative to the Poisson limit marked by the solid line.

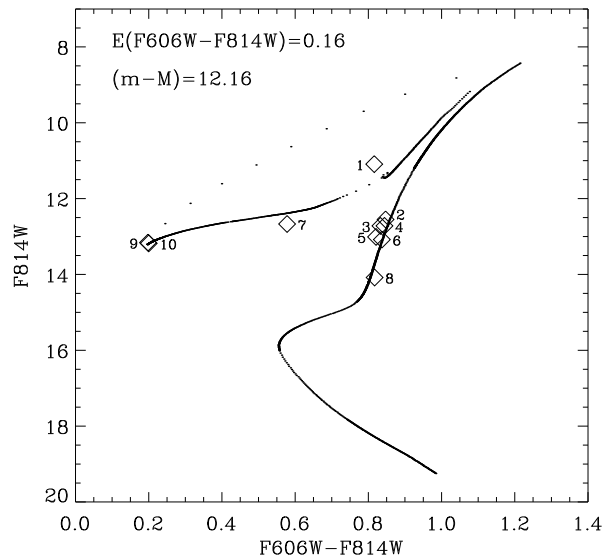


FIG. 3.— Color-magnitude diagram of bright stars in NGC6397, and an overlaid isochrone from the BaSTI grid (see text).

brighter than 14.1 magnitude. Adopting the absolute photometry from Richer et al. (2008) we show in Figure 3 those bright cluster members and an appropriate isochrone from the BaSTI grid (Pietrinferni et al. 2004) for age = 13 Gyr, $Y = 0.245$, and $Z = 0.0001$ corresponding to $[\text{Fe}/\text{H}] = -2.3$. The model uses scaled solar mixture, no overshooting, and assumes a mass loss parameter of $\eta = 0.4$. To match the bright cluster stars with the isochrone we adopted a reddening and distance modulus of $E(F606W - F814W) = 0.18$ and $(m - M)_{F814W} = 12.6$ respectively in agreement with

previous values in the literature (e.g. see Richer et al. (2008) and references therein). We obtained the stellar parameters L/L_{\odot} , T_{eff} and M/M_{\odot} by matching each star to the isochrone. We then estimated the frequency at maximum power, the characteristic frequency spacing between modes of successive radial order, and the mode amplitude using the scaling relations from Kjeldsen & Bedding (1995) and Samadi et al. (2005). The results are listed in Table 1. The first column is the star number, second to fifth columns are x , y , F814W, and F606W-F814W from Table 1 of Richer et al. (2008), columns 6–9 are luminosity, temperature, radius and mass, and the last four columns are expected frequency of maximum power, the characteristic frequency spacing, and the amplitude based on two different scaling relations.

4. TIME-SERIES ANALYSIS

To enhance the signal-to-noise we sought to combine the data obtained through the two filters. Fortunately, there are no phase changes in the solar oscillations observed in different filters with bandpass differences of roughly 200 nm (Jiménez et al. 1999), and we therefore expect the same adiabatic behaviour for high-order solar-like oscillations in other stars. Hence, we combine the data by simply scaling the amplitude of one of the datasets to accommodate the $1/\lambda_{\text{filter}}$ dependence while adjusting their weights to preserve the correct noise level.

Out of the full set of 510 stars power spectra are generally flat, with little evidence of excess low frequency noise coming in as would always be the case with ground-based data. Of the 10 red giants listed in Table 1 we show power spectra (weighted Fourier transform) of the best candidates in Figure 4. These were selected to have a white noise level below 100ppm (in amplitude) and with expected oscillation frequencies below $100\mu\text{Hz}$ to avoid strong aliasing from the orbital frequency of the spacecraft. Due to daily gaps in the data the spectral window is similar to ground-based single-site observations (see inset in top panel).

A quite strong excess of power at low frequencies is seen for star No. 1 consistent with the expected frequencies from solar-like oscillations indicated with a horizontal line. No other star in our sample shows such a steep increase in power towards low frequencies. Note the much larger ordinate range in the top panel. However, the high peaks in this frequency range are only just resolved and do not support a detailed frequency analysis (see § 6).

The rest of the sample show at most a few intriguing peaks. The maximum signal-to-noise ratio (SNR) is 3.8 (in amplitude) between the highest peak and the average level measured in the frequency range 67–87 μHz , denoted n_w in Figure 4 for stars 2–7. Hence, extracting individual peaks from these spectra is barely justified. Instead we look for broad envelopes of excess power by smoothing the spectra and compare that to a Harvey model for the background noise (Harvey 1985). The solid black curve in Figure 5 shows the smoothed power spectra (scaled to power density) and an overlaid one-component Harvey model (dashed curve)

$$p(\nu) = n_w + \frac{4\sigma^2\tau}{1 + (2\pi\nu\tau)^2}, \quad (1)$$

where $p(\nu)$ is the power density at frequency, ν , n_w is

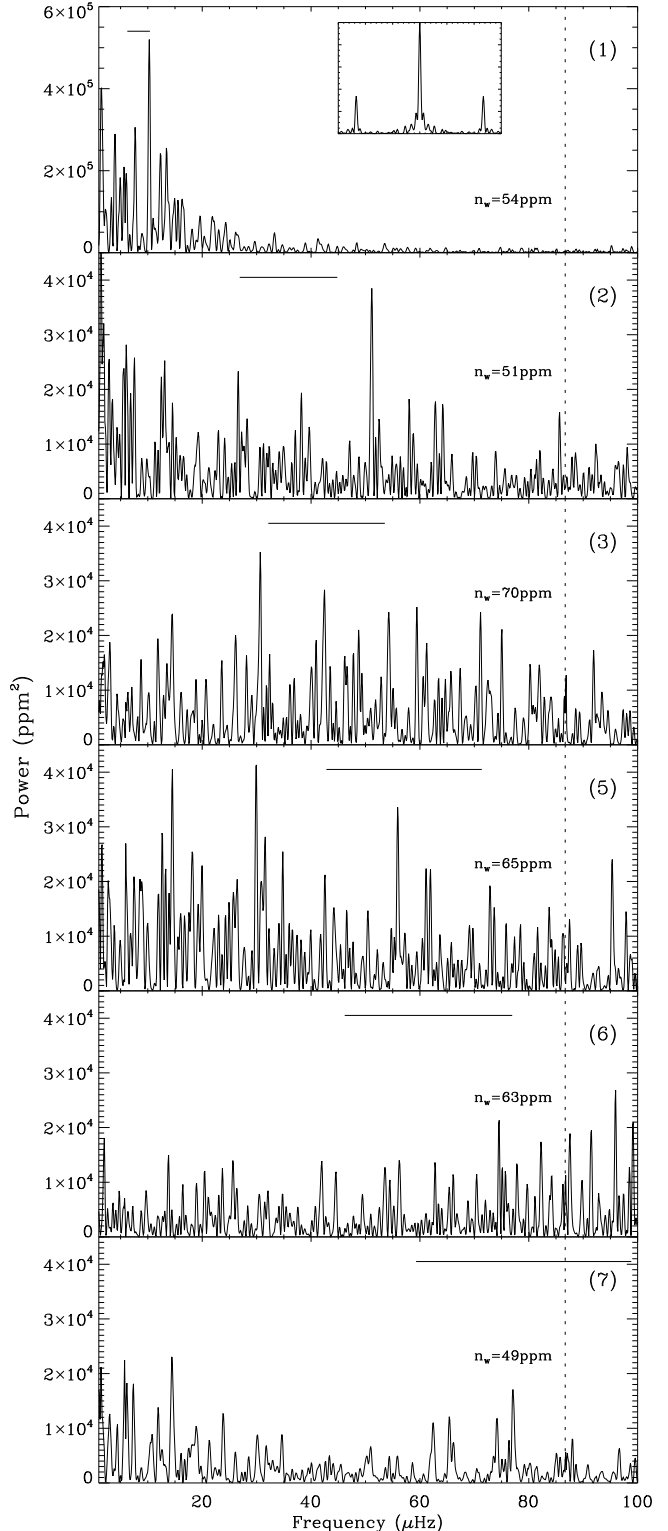


FIG. 4.— Fourier spectra of red giant stars listed in Table 1. The dotted lined indicates half the orbital frequency, and n_w is the mean level in the spectra in the range 67–87 μHz converted to amplitude. The expected frequency range of the oscillations ($\nu_{\text{max}} \pm \frac{1}{2}\nu_{\text{max}}$) is marked by the horizontal bar. The inset in the top panel shows the spectral window on the same frequency scale as the main panel, and is representative for all stars. Star numbers relating to Table 1 are marked in each panel.

TABLE 1
STELLAR PARAMETERS

Star	x	y	F814W	F606W–F814W	L/L_{\odot}	T_{eff}	R/R_{\odot}	M/M_{\odot}	ν_{max}	$\Delta\nu$	L/M	$(L/M)^{0.7}$
(1)	(2)	(3)	(4)	(5)	(6)	(7)	(8)	(9)	(10)	(11)	(12)	(13)
1	1824.0	922.0	11.09	0.816	174	5100	16.9	0.72	8.31	1.65	983	190
2	1881.0	1181.0	12.55	0.847	46.7	5192	8.46	0.79	35.9	4.86	234	68.7
3	552.1	992.0	12.72	0.833	39.8	5219	7.73	0.79	42.8	5.56	197	60.8
4	2186.0	1794.0	12.72	0.844	39.8	5219	7.73	0.79	42.8	5.56	197	60.8
5	923.2	937.0	13.01	0.821	30.8	5262	6.69	0.79	57.1	6.92	150	49.9
6	2097.0	1827.0	13.08	0.837	28.8	5274	6.44	0.79	61.6	7.33	139	47.4
7	2254.0	372.0	12.67	0.578	58.4	7108	5.05	0.72	79.1	10.1	170	45.5
8	1520.0	909.0	14.08	0.817	11.7	5421	3.89	0.79	170	15.6	53.9	23.9
9	1310.0	1506.0	13.16	0.198	48.8	8931	2.92	0.72	210	22.9	90.0	25.4
10	2049.0	1549.0	13.16	0.200	48.8	8931	2.92	0.72	210	22.9	90.0	25.4

(2)–(5) are from Table 1 in Richer et al. (2008)

If mass loss is ignored all the stars would have a mass of roughly $0.79 M_{\odot}$.

the lowest level in the power spectrum (assumed to be dominated by white noise), and σ and τ are the rms amplitude and characteristic time scale for the background, respectively. Smoothing is done by convolving the spectra with a Gaussian function of width $4\Delta\nu$, which follows the approach by Kjeldsen et al. (2008a). For comparison we also show with a dashed curve the average smoothed spectrum of star No. 9 and 10, which both have expected frequencies well beyond the plotted range and very low expected amplitudes. Hence, this serves as a reference where we do not expect any detectable signal from oscillations. There appears to be excess power in five out of these six stars, roughly following the same trend as the estimated ν_{max} (horizontal bar). We note that to some extent the location of the excess humps seen in Figure 5 are reproduced by the ‘‘oscillation-quiet’’ reference stars when the same degree of smoothing is applied. In particular, the spectrum of star No. 8, which was discarded due to its high noise level, looked very similar to what we see for star No. 6, suggesting that its excess hump is a noise feature. This is further supported by its location at half the orbital frequency ($174 \mu\text{Hz}$) of the spacecraft.

5. MODE LIFETIMES AND AMPLITUDES

In the following we use the results from the previous section to estimate the amplitude per mode under the assumption the excess power levels seen in Figure 5 are due to solar-like oscillations. Due to inadequate time resolution and signal-to-noise of our data, the mode lifetimes were not attainable in any of the stars. Hence, we measure the amplitudes following the approach suggested by Kjeldsen et al. (2005), which is independent of mode lifetime. First we subtract the background from the smoothed power density spectrum and multiply with the mean mode spacing. As we do not know whether non-radial modes are excited in these stars, we used the following average mode spacings to bracket the possible range, $\Delta\nu$ if radial modes dominate the spectrum and $\Delta\nu/3$ for a Sun-like case with both radial and non-radial modes taking into account the relative mode visibilities from whole-disk integrated intensity observations (Kjeldsen et al. 2008a). We finally take the square root to get the amplitude. From Figure 6, which shows the result

for star No. 1, we conclude that $(L/M)^{0.7}T_{\text{eff}}^{-2}$ scaling (dot) provides better agreement with our measured amplitude range than does the $LM^{-1}T_{\text{eff}}^{-2}$ scaling. This supports previous findings on metal-poor stars by Bedding et al. (2006) and Frandsen et al. (2007). We performed similar analyses to the other stars with excess power (No. 2, 3, 6, and 7), which provided ambiguous results. While being in agreement with $(L/M)^{0.7}T_{\text{eff}}^{-2}$ scaling, these low levels of excess power were also consistent with being noise.

Recently, Gilliland (2008) derived an amplitude relation calibrated with a large set of red giants in the Galactic bulge observed during seven days with the HST. This relation does not take into account the effect from mode lifetime or length of the time series. While we in the above analysis compared observed amplitude per mode with the theoretical predictions, this relation predicts the rms excess, which Gilliland (2008) calculated relative to ‘quiet’ comparison stars with no detectable oscillation or granulation signal. Hence, $\text{rms}_{\text{excess}} = (\text{rms}_{\text{star}}^2 - \text{rms}_{\text{quiet}}^2)^{0.5}$ is not directly comparable to the two previously discussed amplitude scaling relations. We have no comparison stars of the same magnitude, and use instead the first-difference scatter of the star itself to resemble an intrinsic quiet star, which is similar to calculating the rms of the high-pass filtered time series. This leads to an rms excess for star No. 1 of approximately 700 ppm, which is in quite good agreement with the roughly 600 ppm estimated from equation (5) in Gilliland (2008).

6. REGULAR FREQUENCY SPACINGS

Further evidence that would support the existence of solar-like oscillations in these data would be a regular series of peaks in the power spectrum corresponding to either the large frequency spacing, $\Delta\nu$, if the spectrum is dominated by radial modes or half that if we have significant non-radial modes of degree $l = 1$ as well. Such regular spacing can be revealed by calculating the autocorrelation function across the power spectrum even for very low signal-to-noise cases where the excess power is not directly apparent in the power spectra (Chaplin et al. 2008). We calculated the autocorrelation functions for all six stars shown in Figure 4, but found no compelling evi-

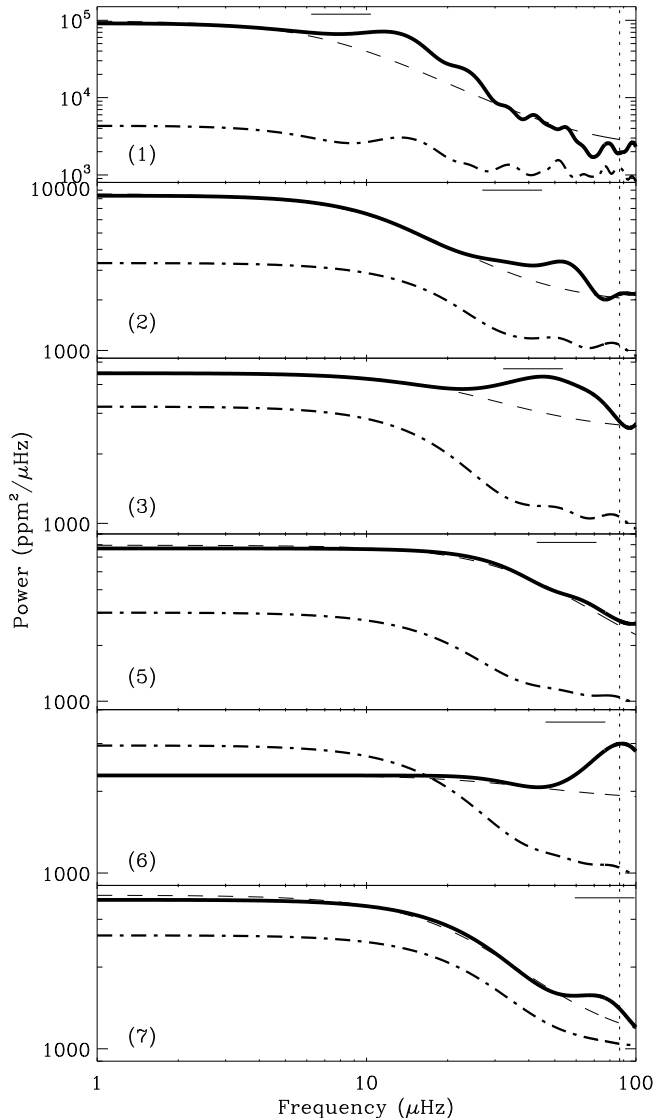


FIG. 5.— Power density spectra of the stars shown in Figure. 4 convolved with a Gaussian with width $4\Delta\nu$. With the same degree of smoothing we show for comparison the average smoothed spectrum of two stars where no detectable oscillations are expected (dash-dot). The dashed line shows a representative one-component Harvey model including a white noise term as shown in equation 1.

dence of regular spacing that were in agreement with the expected $\Delta\nu$. For our most promising star No. 1 the excess power is confined to such a narrow frequency range that the autocorrelation function did not provide robust results. Instead we extracted the eight highest peaks with $\text{SNR} > 4$ relative to the white noise level, which hinted a spacing of about $2.3\mu\text{Hz}$ between five consecutive peaks. This slightly larger than expected frequency spacing is in qualitative agreement with the observed excess power also being at a slightly higher frequency range than expected (see Table 1). However, we are cautious about claiming any detection of a regular series of frequencies because the $2.3\mu\text{Hz}$ spacing is only 2–3 times the general spacing seen between successive peaks in the power spectrum, which implies the spacing is barely resolved, and likely influenced if not possibly caused by the

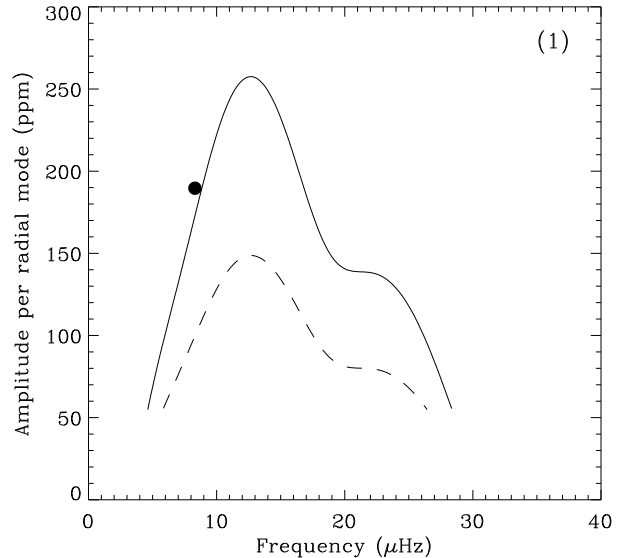


FIG. 6.— Amplitude per radial mode for star No. 1 assuming only radial modes (solid curve) and non-radial modes in addition (dashed curve). The dot marks the predicted ν_{max} and amplitude from scaling relations (Table 1 cols (10) and (13)).

limiting frequency resolution.

7. DISCUSSION

The marginal detections of oscillations in this experiment can largely be attributed to the data acquisition process, which was far from ideal for our purpose due to the large scale dithering, extremely saturated stars, and poor duty cycle. The lowest noise levels reached in an amplitude spectrum for these data are about 50 ppm. For stars at brightness comparable to our star No. 1 ($V \sim 12$) the Kepler Mission (Borucki et al. 2007) will provide 30 minute sampling on stars unsaturated in underlying 6 second co-added exposures, with a Poisson noise level of 65 ppm. With the expectation of near 100% duty cycle a 23 day interval will provide amplitude spectrum noise levels of about 4 ppm, or more than an order of magnitude better than those obtained here. From the CoRoT mission we have already started to see the first glimpse on what to expect from long term monitoring of red giant stars using high-precision space photometry (Hekker et al. 2008; Kallinger et al. 2008b; De Ridder et al. 2009). Coupled with a near perfect window function and observations expected to extend over 3.5 years for some 1000 red giants with $V \sim 12$, the Kepler data will provide several orders of magnitude gain in capability relative to these serendipitously available data from a (non-ideal for our purposes) HST program.

8. CONCLUSION

We used data obtained with the HST over 23 days to search for solar-like oscillations in the red giant population of the metal-poor cluster NGC6397. We found evidence for excess power in the power spectra in agreement with expected frequencies from solar scaling. Except for one star this evidence is tentative due to the low signal-to-noise, and extraction of individual mode frequencies was not justified. As a consequence mode lifetimes and

mode identification was not attainable. For the most promising star (No. 1), the most luminous in our sample, we were able to estimate the amplitude per mode from the excess power, which favours that the amplitude follows a $(L/M)^{0.7}T_{\text{eff}}^{-2}$ relation rather than a $LM^{-1}T_{\text{eff}}^{-2}$ relation when scaled from the Sun. Unfortunately, the frequency resolution of our dataset does not allow convincing verification of the typical solar-like regular series of peaks in the power spectrum. However, these results still represent the best available evidence of solar-like oscillations in such metal-poor stars.

DS acknowledge support from the Australian Research Council. RG acknowledges support through GO/AR-11254 from STScI.

REFERENCES

- Barban, C., Matthews, J. M., de Ridder, J., Baudin, F., Kuschnig, R., Mazumdar, A., Samadi, R., Guenther, D. B., Moffat, A. F. J., Rucinski, S. M., Sasselov, D., Walker, G. A. H., & Weiss, W. W. 2007, *A&A*, 468, 1033
- Bedding, T. R., Butler, R. P., Carrier, F., Bouchy, F., Brewer, B. J., Eggenberger, P., Grundahl, F., Kjeldsen, H., McCarthy, C., Bjorn Nielsen, T., Retter, A., & Tinney, C. G. 2006, *ArXiv Astrophysics e-prints*
- Bedding, T. R., & Kjeldsen, H. 2007, *Communications in Asteroseismology*, 150, 106
- Borucki, W. J., Koch, D. G., Lissauer, J., Basri, G., Brown, T., Caldwell, D. A., Jenkins, J. M., Caldwell, J. J., Christensen-Dalsgaard, J., Cochran, W. D., Dunham, E. W., Gautier, T. N., Geary, J. C., Latham, D., Sasselov, D., Gilliland, R. L., Howell, S., Monet, D. G., & Batalha, N. 2007, in *Astronomical Society of the Pacific Conference Series*, Vol. 366, *Transiting Extrapolar Planets Workshop*, ed. C. Afonso, D. Wel Drake, & T. Henning, 309
- Brown, T. M., Gilliland, R. L., Noyes, R. W., & Ramsey, L. W. 1991, *ApJ*, 368, 599
- Chaplin, W. J., Appourchaux, T., Arentoft, T., Ballot, J., Christensen-Dalsgaard, J., Creevey, O. L., Elsworth, Y., Fletcher, S. T., García, R. A., Houdek, G., Jiménez-Reyes, S. J., Kjeldsen, H., New, R., Régulo, C., Salabert, D., Sekii, T., Sousa, S. G., Toutain, T., & the rest of the asterofLAG group. 2008, *Astronomische Nachrichten*, 329, 549
- De Ridder, J., Barban, C., Baudin, F., Carrier, F., Hatzes, A. P., Hekker, S., Kallinger, T., Weiss, W. W., Baglin, A., Auvergne, M., Samadi, S., Barge, P., & Deleuil, M. 2009, *nature*, accepted
- De Ridder, J., Barban, C., Carrier, F., Mazumdar, A., Eggenberger, P., Aerts, C., Deruyter, S., & Vanautgaerden, J. 2006, *A&A*, 448, 689
- Edmonds, P. D., & Gilliland, R. L. 1996, *ApJ*, 464, L157
- Frandsen, S., Bruntt, H., Grundahl, F., Kopacki, G., Kjeldsen, H., Arentoft, T., Stello, D., Bedding, T. R., Jacob, A. P., Gilliland, R. L., Edmonds, P. D., Michel, E., & Matthesen, J. 2007, *A&A*, 475, 991
- Frandsen, S., Carrier, F., Aerts, C., Stello, D., Maas, T., Burnet, M., Bruntt, H., Teixeira, T. C., de Medeiros, J. R., Bouchy, F., Kjeldsen, H., Pijpers, F., & Christensen-Dalsgaard, J. 2002, *A&A*, 394, L5
- Gilliland, R. L. 2008, *AJ*, 136, 566
- Gilliland, R. L., Brown, T. M., Kjeldsen, H., McCarthy, J. K., Peri, M. L., Belmonte, J. A., Vidal, I., Cram, L. E., Palmer, J., Frandsen, S., Parthasarathy, M., Petro, L., Schneider, H., Stetson, P. B., & Weiss, W. W. 1993, *AJ*, 106, 2441
- Hansen, B. M. S., Anderson, J., Brewer, J., Dotter, A., Fahlman, G. G., Hurley, J., Kalirai, J., King, I., Reitzel, D., Richer, H. B., Rich, R. M., Shara, M. M., & Stetson, P. B. 2007, *ApJ*, 671, 380
- Harvey, J. 1985, in *ESA SP-235: Future Missions in Solar, Heliospheric & Space Plasma Physics*, ed. E. Rolfe & B. Battrock, 199
- Hatzes, A. P., & Zechmeister, M. 2007, *ApJ*, 670, L37
- Hekker, S., Barban, C., Kallinger, T., Weiss, W., de Ridder, J., Hatzes, A., & COROT Team. 2008, *Communications in Asteroseismology*, 157, 319
- Houdek, G., & Gough, D. O. 2002, *MNRAS*, 336, L65
- Jiménez, A., Roca Cortés, T., Severino, G., & Marmolino, C. 1999, *ApJ*, 525, 1042
- Kallinger, T., Guenther, D. B., Matthews, J. M., Weiss, W. W., Huber, D., Kuschnig, R., Moffat, A. F. J., Rucinski, S. M., & Sasselov, D. 2008a, *A&A*, 478, 497
- Kallinger, T., Weiss, W. W., Barban, C., Baudin, F., Carrier, F., De Ridder, J., Hatzes, A., Hekker, S., & Deleuil, M. 2008b, *ArXiv e-prints*
- Kjeldsen, H., & Bedding, T. R. 1995, *A&A*, 293, 87
- Kjeldsen, H., & Bedding, T. R. 2004, in *ESA Special Publication*, Vol. 559, *SOHO 14 Helio- and Asteroseismology: Towards a Golden Future*, ed. D. Danesy, 101
- Kjeldsen, H., Bedding, T. R., Arentoft, T., Butler, R. P., Dall, T. H., Karoff, C., Kiss, L. L., Tinney, C. G., & Chaplin, W. J. 2008a, *ApJ*, 682, 1370
- Kjeldsen, H., Bedding, T. R., Butler, R. P., Christensen-Dalsgaard, J., Kiss, L. L., McCarthy, C., Marcy, G. W., Tinney, C. G., & Wright, J. T. 2005, *ApJ*, 635, 1281
- Kjeldsen, H., Bedding, T. R., & Christensen-Dalsgaard, J. 2008b, *ApJ*, 683, L175
- Pietrinferni, A., Cassisi, S., Salaris, M., & Castelli, F. 2004, *ApJ*, 612, 168
- Richer, H. B., Dotter, A., Hurley, J., Anderson, J., King, I., Davis, S., Fahlman, G. G., Hansen, B. M. S., Kalirai, J., Paust, N., Rich, R. M., & Shara, M. M. 2008, *AJ*, 135, 2141
- Samadi, R., Goupil, M.-J., Alecian, E., Baudin, F., Georgobiani, D., Trampedach, R., Stein, R., & Nordlund, Å. 2005, *JApA*, 26, 171
- Stello, D., Bruntt, H., Kjeldsen, H., Bedding, T. R., Arentoft, T., Gilliland, R. L., Nuspl, J., Kim, S.-L., Kang, Y. B., Koo, J.-R., Lee, J.-A., Sterken, C., Lee, C.-U., Jensen, H. R., Jacob, A. P., Szabó, R., Frandsen, S., Csubry, Z., Dind, Z. E., Bouzid, M. Y., Dall, T. H., & Kiss, L. L. 2007, *MNRAS*, 377, 584
- Stello, D., Bruntt, H., Preston, H., & Buzasi, D. 2008, *ApJ*, 674, L53
- Stello, D., Kjeldsen, H., Bedding, T. R., & Buzasi, D. 2006, *A&A*, 448, 709